平成１０年度石田記念財団研究助成研究成果報告書

電子サイクロトロン共鳴によるプラズマの局所構造制御

東北大学大学院工学研究科電子工学専攻　　畠山力三

１．はじめに

情報通信などの電波応用技術の今日的発展に、マイクロ波あるいはミリ波帯の電磁波動が大きな役割を果たしてきたことは論をまたない。また、この領域の電磁波動は近年では、宇宙規模の情報通信の開拓、新材料開発、未来エネルギー開発のいずれの研究にも深く関与して重要な、物質の第四状態としての「正と負の荷電粒子集団“プラズマ”」の内部情報計測手段としても活用されている。

一方、筆者らは最近、、プラズマの先進的応用を展開するためにその局所構造を制御する手段として、マイクロ波－ミリ波帯（1～150 GHz）の高周波電磁場を用いる研究を行ってきている。これまで得られている研究成果を以下に概説する。

２．プラズマ局所構造制御の原理

一般に、磁化プラズマ中電子の旋回運動周波数に一致する周波数をもつ高周波電磁場を印加すると、電子は磁場に垂直方向に共鳴的に加速され（電子サイクロトロン共鳴、ＥＣＲ）、加熱に至る（ＥＣＲＨ）。従って、その強度が空間的に変化している不均一磁場中に（B=0.5～50 kG）存在するプラズマに対して、マイクロ波－ミリ波帯の高周波を印加すると、電子のみが垂直方向に局所的な加速・加熱を受けた後に、磁場勾配力により磁力線方向に加速または減速されることになる。しかし、質量の重いイオンはその高周波の影響を直接的には受けない。しかるに、プラズマは電気的に準中性を維持しようとする性質を本質的に持っているので、自発的に静電ポテンシャルが形成され、これがイオンを電子と同じく磁力線方向に加速または減速するように働く。その結果、局所的に電子及びイオンの双方の粒子の流れと熱の流れを、磁場勾配の符号に応じて促進あるいは阻止するようなプラズマ構造が形成されることになる。

３．実験結果とシミュレーション結果のまとめ

以上の考察の上にそのシナリオを証明するために、東北大学のＱマシンと呼ばれる直線型の装置を用いて基礎実験を行った。

局所的に井戸型（下図の上絵を参照）、または正の磁場勾配をもつ収束型（下図の中絵）不均一磁場配位中に電子とカリウム正イオンK^+から成る完全電離無衝突プラズマを流し込み、そこに 6GHz のマイクロ波を入射し局所ＥＣＲを発生させた。その結果、電子を反射できる程度の深さをもつ電位窪み$\Delta\phi_d$とそれに後続してイオン流を阻止できる程度の高さをもつ電位隆起$\Delta\phi_p$から成る二重構造の静電ポテンシャルϕが形成され（下図の絵）、プラズマ流の堰き止めダム（サーマルバリア・プラグ電位と呼ぶ）が実現されていることが明らかになった。この成果は、井戸型磁場配位については添付資料Ⅰ（５～８ページ）に、収束型磁場配位については添付資料Ⅱ（９～１３ページ）に詳しく収録されている。

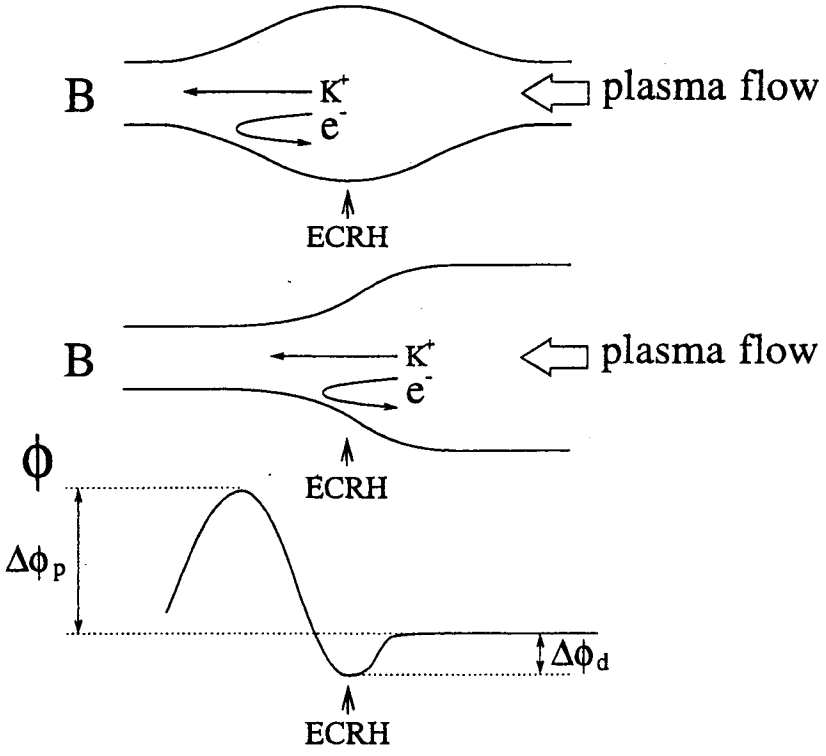

さらに、局所的に負の磁場勾配をもつ発散型磁場配位（次ページの図の上絵）中の実験では、局所ＥＣＲにより逆の静電ポテンシャル分布が形成され（次ページの図の下絵）、イオンが磁力線方向に有効的に加速されていることが明らかにされた。その成果は、添付資料Ⅲ（１４～１８ページ）に詳しく収録されている。

これらの成果は、プラズマ理工学国際会議の招待講演として総合的に報告され大きな注目を引いた。また、局所井戸型磁場配位における唯一点のみのＥＣＲによる二重構造静電ポテンシャル形成の成果は、次世代エネルギー開発のキーポイントである高効率プラズマ閉じこめを可能にする“サーマルバリア・タンデムポテンシャル”形成を極めて

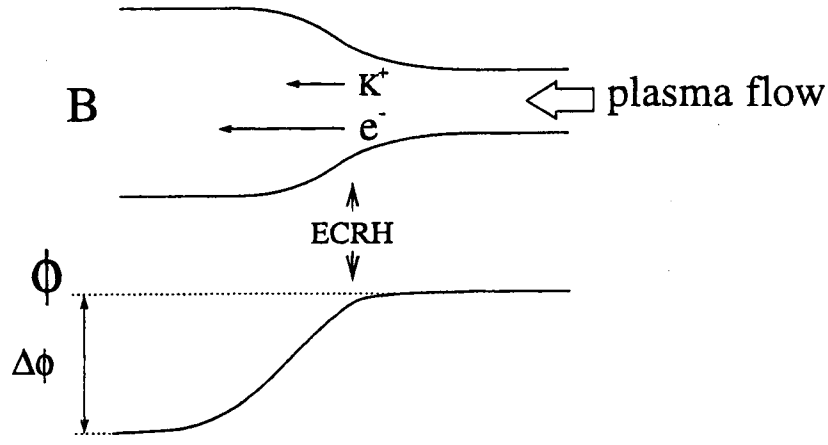

単純に実現したものとして、米国物理学会誌にトピックス的に掲載され大きな反響を呼んでいる。

このような実験結果の電位構造形成機構をより詳細に解明するために、２次元静電ＰＩＣ計算機シミュレーションによる研究も開始され、実験では測定できなかった興味深い物理的過程が理解されつつあるが、これに関する添付資料をここでは割愛する.

また最近では、マイクロ波が、アンテナから不均一磁場中を経て局所電子サイクロトロン共鳴を起こしプラズマ構造形成に至る過程を、線形・非線形波動伝搬の立場から詳細に解明する研究を精力的に行っている。その初期成果は、添付資料Ⅳ（１９ページ）にやや詳しく収録されている。これが明らかになれば、電子サイクロトロン共鳴によるプラズマの局所構造制御の他の応用、例えばプラズマ不安定性の抑制などへの応用への道が拓けるものと期待される。

４．おわりに

電波通信に重要な電離層には物質の第四状態としてのプラズマが存在するが、プラズマには未来エネルギー開発等への様々な応用の可能性が秘められている。本研究においては、マイクロ波帯の電磁波を用いる不均一磁場中の電子サイクロトロン共鳴効果により、高効率閉じ込め等を可能にするプラズマの局所電位構造を制御することに成功した。

５．研究発表

1) T. Kaneko, R. Hatakeyama ,and N. Sato, “Potential Formation Due to ECR under Mirror Configurations of Magnetic Field”, Plasma Phys. Control. Fusion **39**, (1997) A129.

2) T. Kaneko, R. Hatakeyama, and N. Sato, "Potential Structure Modified by Electron Cyclotron Resonance in a Plasma Flow along Magnetic Field Lines with Mirror Configuration", Phys. Rev. Lett. 80, (1998) 2602.

3) N. Sato, R. Hatakeyama, T. Kaneko *et. al.*, "Control of Parallel and Perpendicular Potential Profiles in Open-Ended Plasma Confinement Systems", *Proceedigs of 17th IAEA Fusion Energy Conference* (1998) 162.

4) 金子俊郎，石黒青児，畠山力三，佐藤徳芳、"局所ＥＣＲによるプラズマ電位形成のシミュレーション"，プラズマ・核融合学会第１５回年会，筑波大学，１９９８年１２月３日.

5) R. Hatakeyama, T. Kaneko, and N. Sato, "Plasma Potential Formation and Particle Acceleration Due to ECRH in Diverging Magnetic-Field Lines", Trans. Fusion Technol. 35, (1999) 325.

6) T. Kaneko, Y. Miyahara, R. Hatakeyama, and N. Sato, "Formation of Plasma-Flow Dike Potential Due to Local ECR along Converging Magnetic-Field Lines", Trans. Fusion Technol. 35, (1999) 335.

7) 金子俊郎，石黒静児，畠山力三，佐藤徳芳，"ミラー磁場中局所ＥＣＲに伴う電位形成シミュレーション"，日本物理学会第５４回年会，広島大学，１９９９年3月３１日.

8) 高橋護，金子俊郎，畠山力三，佐藤徳芳，"局所ＥＣＲによるプラズマ電位形成の計算機シミュレーション"，平成１１年度電気関係学会東北支部連合大会，１９９９年8月１９日.

9) 金子俊郎，石黒青児，畠山力三，佐藤徳芳，"不均一磁場中局所ＥＣＲにより形成されるプラズマ電位構造の解析"，プラズマ・核融合学会第１６回年会，東北大学，１９９９年１１月２５日.

10) 村井宏一，金子俊郎，畠山力三，佐藤徳芳，"不均一磁場中ＥＣＲに関与する波動伝播"，プラズマ・核融合学会第１６回年会，東北大学，１９９９年１１月２５日.

添付資料 I （井戸型磁場配位）

Potential Structure Modified by Electron Cyclotron Resonance in a Plasma Flow along Magnetic Field Lines with Mirror Configuration

T. Kaneko, R. Hatakeyama, and N. Sato

Department of Electronic Engineering, Tohoku University, Sendai 980-8579, Japan

(Received 21 July 1997)

A plasma potential structure is modified by the electron cyclotron resonance (ECR) in a collisionless plasma flow along magnetic field lines with simple mirror configuration. In the presence of a single ECR point at the bottom of the magnetic well, there appears a potential dip (thermal barrier) around this point, being followed by a potential hump (plug potential) in the downstream side. The result in this simplified configuration gives a clear-cut physics to the formation of field-aligned plug potential with thermal barrier. [S0031-9007(98)05529-X]

PACS numbers: 52.58.Qv, 52.35.Nx, 52.50.Gj, 52.55.Jd

Plasma-potential formation in inhomogeneous magnetic fields is of great interest in conjunction with field-aligned particle acceleration, plasma confinement, and heat-transport reduction. In space plasmas, a field-aligned potential difference has been predicted to be generated by different pitch-angle anisotropies of electrons and ions along converging magnetic field lines [1], which was demonstrated in particle simulations [2] and in laboratory experiments [3]. The field-aligned potential difference due to double layers [4] has been proposed to play an important role in the aurora phenomena which have often been accompanied by intense wave emissions around the local electron cyclotron frequency [5]. In fusion-oriented plasmas, concepts of a plug potential with thermal barrier (plug/barrier potential) [6] and a thermal dike [7] have been proposed in order to realize the plasma confinement necessary for tandem-mirror devices and to reduce the heat transport in tokamak divertors, respectively. According to the original tandem-mirror scenario for the plug/barrier potential formation [8,9], a neutral beam injection (NBI) producing sloshing ions is necessary, in addition to the electron cyclotron resonances (ECR) at two positions with different magnetic fields in the end mirror cells. The recent experiment on the GAMMA 10 [10], however, indicates that this potential structure is formed without NBI in the presence of the two ECR points, although a physical mechanism of the potential formation has been unsolved. Actually, it is difficult to measure the overall field-aligned potential profiles in such a big fusion-oriented mirror device as the GAMMA 10 [8–11], and, thus, it has long been claimed to make an investigation under a simplified situation to clarify an essential mechanism of the potential formation due to the ECR.

In the presence of the ECR under a magnetic mirror field, the field-aligned magnetic force, $-\mu\nabla B$, acting on electrons increases, enhancing the electron trapping in the magnetic well, where μ is the magnetic moment of electrons and ∇B is the gradient of B in the direction parallel to magnetic field lines. Then, there appears an electrostatic force acting on ions under the condition of charge neutrality. This mechanism provides a straightforward formation of a plug potential with thermal barrier in a plasma flowing along magnetic field lines with mirror configuration. Here we demonstrate this simple scenario for the plug/barrier formation. The physics of plug-potential formation is the same as that in the double-layer formation triggered by a small potential dip in current-carrying plasmas [12]. In our paper, in contrast to the double-layer formation, the scale length is much larger and the potential dip is produced by the mirror trapping of electrons in the plasma flow without electric current.

A plasma is produced by surface ionization of potassium atoms on a 5.0-cm-diam hot tungsten plate under an electron-rich condition and is confined by a magnetic field B of a few kG in a single-ended Q machine [13], as shown schematically in Fig. 1. Ions are accelerated by a potential drop of the electron sheath in front of the hot plate which is grounded electrically, together with a 20.8-cm-diam vacuum chamber. There is a grid (0.03-mm-diam wire, 50 mesh/in.) at a distance of 40 cm from the hot plate, which is biased negatively with respect to the hot plate. A step potential ϕ_g is applied to the grid so as to increase the grid potential up to the plasma potential in order to inject a plasma flow along the magnetic field [3]. A small Langmuir probe is used to measure plasma parameters and their axial profiles. Under our

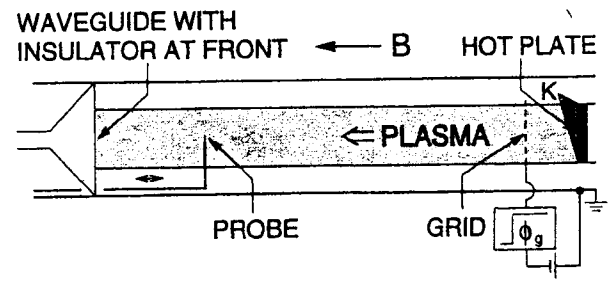

FIG. 1. Schematic of experimental setup. A plasma column, 5 cm in diameter and 310 cm long, is produced by surface ionization.

 0031-9007/98/80(12)/2602(4)$15.00

conditions, the plasma density $n_{p0} \approx 1 \times 10^9$ cm^{-3}, the electron temperature $T_{e0} \approx 0.2$ eV, the ion temperature $T_{i0} \leq T_{e0}$, and the ion flow energy $E_{i0} \approx 10T_{e0}/e$. A background gas pressure is 4×10^{-7} Torr. The plasma is collisionless in the sense that collision mean free paths of electrons and ions are longer than the plasma length.

The experiment is carried out under a simple magnetic mirror configuration which is shown in the top figure in Fig. 2. The bottom of the magnetic well is located at the machine center ($z = 0$ cm). Mirror ratios R_d and R_u in the downstream ($z < 0$) and upstream ($z > 0$) regions are defined as ratios of B around $z = -70$ cm and $z = 100$ cm, respectively, to that at $z = 0$ cm. A microwave with frequency $\omega/2\pi = 6$ GHz and power $P_\mu = 0$–1 W is launched into the plasma through a circular waveguide. The window of the waveguide is covered with an insulator which terminates the plasma column at $z = -150$ cm. The microwave propagates toward the hot plate ($z = 160$ cm) in the region of $\omega/\omega_{ce} < 1$ and the ECR takes place in the vicinity of $\omega/\omega_{ce} = 1$ ($\omega_{ce}/2\pi$: electron cyclotron frequency) at $z = 0$ cm (other situations are found in Ref. [14]). A subscript 0 stands for the parameters in the case of $P_\mu = 0$ W. Time resolved measurements are made by using a usual box-car sampling technique with time resolution of about 1 μs, where probe-current pulses are averaged in a synchronous detection mode.

A typical example of the results in this experiment is presented in Fig. 2. Here, the plasma flow is injected at $t = 0$ ms along the magnetic field with $R_d = 1.68$ and $R_u = 1.30$ for $P_\mu = 0$ W (dotted lines) and 0.5 W (solid lines). J_{es} is the electron saturation current of the probe, which is proportional to the electron density multiplied by the electron thermal speed, and ϕ is the plasma potential. The axial J_{es} and ϕ profiles at the radial center, which are shown at $t = 0.6$ ms in this figure, demonstrate clearly that the plasma flow is almost plugged by the potential structure produced by the ECR. This drastic plugging is also observed for the profiles of the plasma density obtained from J_{es}. The potential structure consists of a potential dip $\Delta\phi_d(<0)$ formed at $z \approx 0$ cm and a subsequent potential hump $\Delta\phi_p(>0)$ along the plasma flow. Here, $\Delta\phi_d$ and $\Delta\phi_p$ are measured with respect to the potential in the upstream region, where ϕ is almost constant spatially, being independent of P_μ.

In Fig. 3, we present temporal evolutions of the J_{es} (solid lines) and ϕ (solid lines with closed circles) profiles under the same conditions as in Fig. 2. Once the plasma front arrives at the ECR region, a clear increase of J_{es} in the ECR region and a drastic decrease of J_{es} in the downstream region appear together with a formation of the potential dip followed by the potential hump along

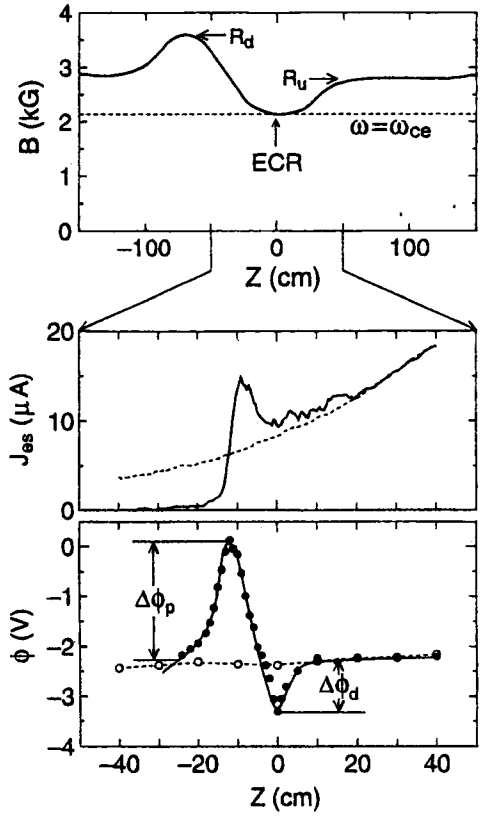

FIG. 2. A typical example of plasma flow plugging due to the ECR, together with magnetic field configuration. This shows profiles of J_{es} (electron saturation current of the probe) and ϕ (plasma potential) at $t = 0.6$ ms in the plasma flow injected at $t = 0$ ms along the magnetic field with $R_d = 1.68$ and $R_u = 1.30$ for $P_\mu = 0$ W (dotted lines) and 0.5 W (solid lines).

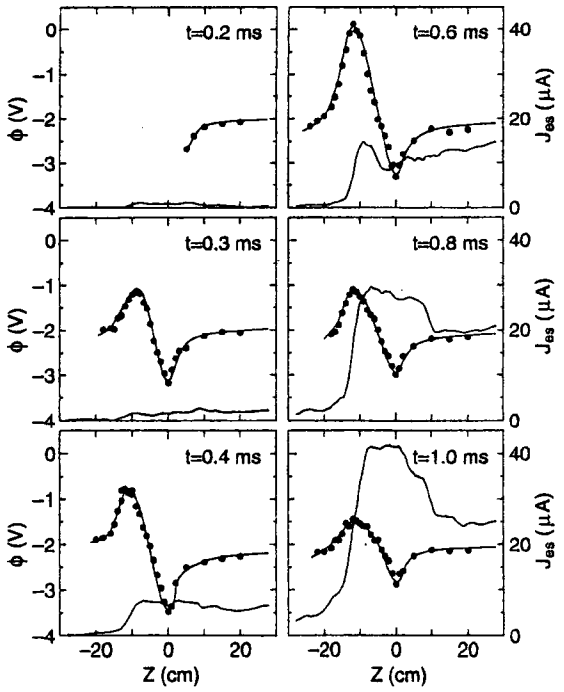

FIG. 3. Temporal evolutions of J_{es} (solid lines) and ϕ (solid lines with closed circles) profiles after the plasma flow is injected at $t = 0$ ms for $P_\mu = 0.5$ W.

the plasma flow. After the potential dip ($\approx -6T_{e0}/e$) is formed at $t = 0.2$–0.3 ms, $\Delta\phi_d$ is found to decrease temporally, gradually approaching a constant value ($\approx -4T_{e0}/e$). On the other hand, the value of $\Delta\phi_p$ has the maximum ($\approx 10T_{e0}/e$) at $t \approx 0.6$ ms which corresponds to the time necessary for the ion flow to arrive at the potential-hump position. At $t > 0.6$ ms, $\Delta\phi_p$ decreases temporally and approaches a constant value ($\approx 3T_{e0}/e$) at $t \approx 1.0$ ms. On the other hand, J_{es} at $z \approx 0$ cm increases monotonously, approaching a constant value at $t \approx 1.0$ ms. This decrease in $\Delta\phi_p$ during the increase in J_{es} is ascribed to a change of the plasma in the upstream region after the ion reflection due to $\Delta\phi_p$. The ion reflection results in a reduction of the plasma flow speed, and then a smaller value of $\Delta\phi_p$ can be sufficient for plugging the plasma flow. There appear density fluctuations of $\tilde{n}_p/n_p = 0.1$–0.2, especially at $t \geq 0.6$ ms in our simple mirror geometry, which might also give rise to a decrease in the flow speed.

The potential structures at the time $t = 0.6$ ms, when $\Delta\phi_p$ has the maximum value, are presented with P_μ as a parameter in Fig. 4, where $R_d = 1.68$ and $R_u = 1.30$. For $P_\mu = 0$ W, a small potential dip ($\approx -T_{e0}/e$) is recognized in the magnetic well, agreeing with the result in Ref. [15]. In the case of $P_\mu \neq 0$ W; however, even for $P_\mu = 0.1$ W, there appears a clear modification of the potential structure. An increase in T_e is also observed at about $z \approx 0$ cm for $P_\mu \neq 0$ W.

Dependences of $\Delta\phi_p$ and $\Delta\phi_d$ on P_μ at $t = 0.6$ ms are presented for $R_d = 1.68$ and $R_u = 1.30$ in Fig. 5(a). With an increase in P_μ, both $\Delta\phi_p$ and $-\Delta\phi_d$ increase, gradually saturating for $P_\mu > 0.5$ W. For $P_\mu = 0.8$ W, we have $e\Delta\phi_d \approx -7\ T_{e0}$ and $e\Delta\phi_p \approx 12\ T_{e0}$, which is of the order of the ion flow energy E_{i0}. T_e at $z \approx 0$ cm increases in a quite similar way and yields a large difference of T_e between the upstream and downstream regions. $T_e \approx 40T_{e0}$ and $e\Delta\phi_p \approx 0.3T_e$ are found for $P_\mu \approx 0.8$ W. This T_e increase, due to the ECR, is confirmed by a modified directional energy analyzer to be dominant in the direction perpendicular to the magnetic field, resulting in the anisotropic electron temperature. The perpendicular electron temperature is a key factor which links $\Delta\phi_p$ with P_μ, as found in the experiment on GAMMA 10 [16].

In Fig. 5(b), $\Delta\phi_p$ and $-\Delta\phi_d$ are plotted as a function of R_d at $t = 0.6$ ms for $P_\mu = 0.8$ W, where $R_d \geq R_u > 1$ is kept. Both $\Delta\phi_p$ and $-\Delta\phi_d$ increase with an increase in R_d, being followed by a gradual saturation. An effect of R_u on the potential formation is also measured at $R_d = 1.68$. But no appreciable changes of $\Delta\phi_p$ and $-\Delta\phi_d$ are observed even when R_u (>1) is increased up to 1.68, indicating that the results are independent of R_u as far as $R_d \geq R_u > 1$ is kept. Thus, we can obtain almost the same results as in Fig. 5(b) even with keeping $R_d = R_u$ (>1) (mirrors are symmetric with respect to $z = 0$ cm).

The increase in P_μ and/or R_d enhances the T_e anisotropy and electron trapping around the ECR point, and thus $-\Delta\phi_d$ increases, being accompanied by an increase in $\Delta\phi_p$ under the charge neutrality condition. Furthermore, $\Delta\phi_p$ always saturates gradually around E_{i0}/e, plugging most of the ions so as not to pass through the magnetic well region. This is because the electrons

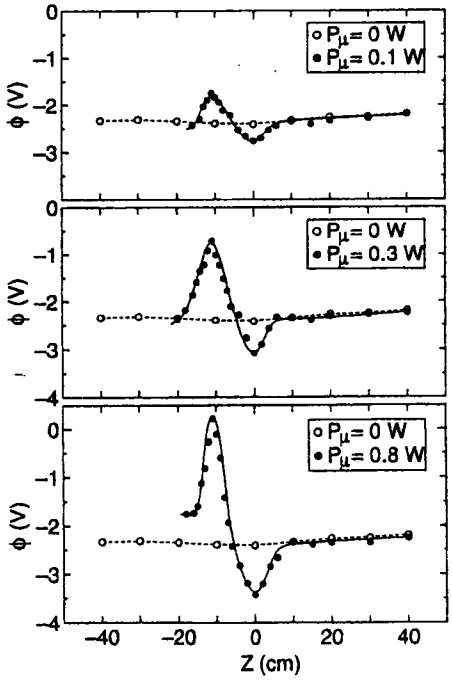

FIG. 4. Spatial profiles of ϕ at $t = 0.6$ ms with P_μ as a parameter in the case of $R_d = 1.68$ and $R_u = 1.30$.

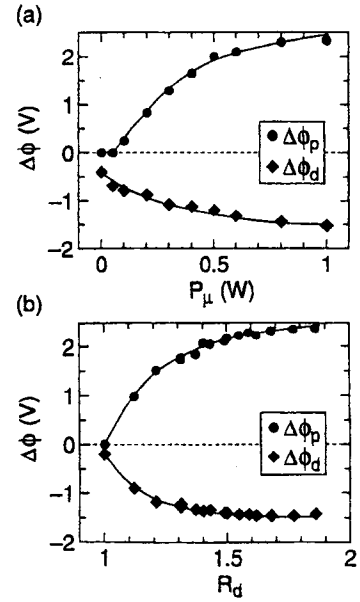

FIG. 5. Potential dip $\Delta\phi_d$ and hump $\Delta\phi_p$ at $t = 0.6$ ms (a) as a function of P_μ for $R_d = 1.68$ and $R_u = 1.30$ and (b) as a function of R_d ($\geq R_u > 1$) for $P_\mu = 0.8$ W.

are well trapped and $-\Delta\phi_d$ is large enough for most of the electrons to be reflected.

As described above, the potential structure observed consists of a potential dip around the ECR point and a subsequent potential hump along the plasma flow. This structure is almost the same as that in the tandem-mirror scenario with the dual ECR performance in the end mirror cells. In our experiment, the electrons accelerated by the ECR in the direction perpendicular to the magnetic field are decelerated and reflected by $-\mu\nabla B$ in the axial direction. The electrons reflected, which are again accelerated at the ECR point, cannot return to the upstream region, being trapped in the magnetic well. This mirror trapping of electrons induces the potential dip around the ECR point. The depth is large enough to prevent cold electrons, which are supplied from the hot plate, from merging with hot electrons in the ECR region. Thus, the potential dip formed works as a "thermal-barrier" potential. Ions are not directly affected by the ECR. But, in order to satisfy the charge neutrality condition, a potential hump, a so-called "plug" potential, the height of which is large enough to reflect most of the ions flowing along the magnetic field lines, is formed in the downstream side. As a result, there appears a density decrease in the downstream region, i.e., the potential structure produced provides a "dike" potential against the plasma flow.

Our physics of the barrier/plug potential formation can also be applied to plasmas with the ion flow energy much smaller than the ion temperature. In this case, however, the flow energy E_{i0} has to be replaced by the ion temperature T_i parallel to the magnetic field. It is to be remarked that $\Delta\phi_p/E_{i0}$ observed in our work is of the same order of $\Delta\phi_p/T_i$ in the GAMMA 10 experiment, although $\Delta\phi_p$ and E_{i0} in the Q machine are much smaller than $\Delta\phi_p$ and T_i in such a big fusion-oriented device as the GAMMA 10.

In conclusion, in a collisionless plasma flow under a simple magnetic mirror configuration, a potential structure with a potential dip followed by a subsequent potential hump is formed by the ECR at the bottom of the magnetic well. Our experiment clearly demonstrates a formation of the plug potential with thermal barrier under a quite simple axisymmetric mirror configuration. The mechanism of the potential formation is based on the electron heating and trapping due to the ECR in the magnetic well under the charge neutrality condition. It is not necessary in our potential formation to take into account the conventional scenario for the tandem-mirror devices, which needs two ECR points: the one for barrier formation and the other for plug formation. In our experiment, a single ECR point is sufficient to provide the plug/barrier potential structure. This work gives a clear physics to the formation of field-aligned plug potential with thermal barrier in a quite simplified way.

We thank Professor M. Inutake for his useful discussions and comments. Discussions with many scientists in the GAMMA 10 group were also fruitful. The authors are indebted to Y. Miyahara and H. Ishida for their assistance. The work was supported by a Grant-in-Aid for Scientific Research from the Ministry of Education, Science, Sports, and Culture, Japan.

[1] H. Alfvén and C.-G. Fälthammar, *Cosmical Electrodynamics* (Oxford University Press, London, 1963), 2nd ed., p. 162.
[2] Y. Serizawa and T. Sato, Phys. Fluids **29**, 2753 (1986); S. Ishiguro *et al.*, Phys. Plasmas **2**, 3271 (1995).
[3] N. Sato *et al.*, Phys. Rev. Lett. **61**, 1615 (1988).
[4] A. Alfvén and P. Carlqvist, Solar Phys. **1**, 220 (1967).
[5] A. Bahnsen *et al.*, J. Geophys. Res. **94**, 6643 (1989); M. Malingre *et al.*, Geophys. Res. Lett. **91**, 1339 (1992).
[6] D.E. Baldwin and B.G. Logan, Phys. Rev. Lett. **43**, 1318 (1979).
[7] T. Ohkawa *et al.*, Phys. Rev. Lett. **51**, 2101 (1983); T. Ohkawa, Kakuyugo Kenkyu (Japan) **64**, 305 (1990).
[8] D.P. Grubb *et al.*, Phys. Rev. Lett. **53**, 783 (1984).
[9] M. Inutake *et al.*, Phys. Rev. Lett. **55**, 939 (1985).
[10] T. Tamano, Phys. Plasmas **2**, 2321 (1995).
[11] C.P. Chang *et al.*, Phys. Fluids **31**, 123 (1988).
[12] T. Sato and H. Okuda, Phys. Rev. Lett. **44**, 740 (1980); C. Chan *et al.*, Phys. Rev. Lett. **52**, 1782 (1984).
[13] R.W. Motley, *Q Machines* (Academic, New York, 1975); N. Sato *et al.*, Phys. Rev. Lett. **34**, 931 (1975).
[14] T. Kaneko *et al.*, Plasma Phys. Control. Fusion **39**, A129 (1997).
[15] Y. Suzuki *et al.*, J. Phys. Soc. Jpn. **55**, 1568 (1986).
[16] T. Saito *et al.*, in *Proceedings of the International Conference on Open Plasma Confinement Systems for Fusion, Novosibirsk, 1993*, edited by A.A. Kabantsev (Budker Institute of Nuclear Physics, Novosibirsk, 1993), p. 121.

添付資料 II （収束型磁場配位）

FORMATION OF PLASMA-FLOW DIKE POTENTIAL DUE TO LOCAL ECR ALONG CONVERGING MAGNETIC-FIELD LINES

Toshiro Kaneko
Graduate School of Engineering
Tohoku University
Sendai 980-8579, Japan
+81-22-217-7129

Yutaka Miyahara
Graduate School of Engineering
Tohoku University
Sendai 980-8579, Japan
+81-22-217-7113

Rikizo Hatakeyama
Graduate School of Engineering
Tohoku University
Sendai 980-8579, Japan
+81-22-217-7045

Noriyoshi Sato
Graduate School of Engineering
Tohoku University
Sendai 980-8579, Japan
+81-22-217-7112

ABSTRACT

The formation of a plasma potential is experimentally investigated in a fully-ionized collisionless plasma flow along converging magnetic-field lines in the presence of a single ECR point. When the ECR occurs in the region of converging region, the potential profile is observed to be drastically modified. The resultant potential structure consists of a negative potential dip and a subsequent positive potential hump working as a plasma-flow dike potential, which persists in the steady state when the ECR point is located in a region of good curvature of the magnetic configuration. However, this potential structure temporally collapses when the ECR point is located in a bad curvature region. The phenomenon is considered to be caused by low-frequency flute and drift instabilities.

I. INTRODUCTION

A series of studies have been made on electrostatic potential formation along inhomogeneous magnetic field lines theoretically,[1] numerically[2] and experimentally.[3] As concerns improvement of particle and energy confinements in a open-ended device, a concept of tandem mirror[4] has been proposed as a means to plug ions. In the original tandem mirror proposals, use of neutral beam injection (NBI) producing sloshing ions and the electron cyclotron resonances (ECR) at two positions with different magnetic fields is considered to form the plug/barrier potentials.[5,6] However, it has recently been reported that the formation of these potentials can be made without NBI.[7] Furthermore, a basic experiment in a laboratory plasma demonstrates that a single ECR point at the bottom of the magnetic well is sufficient to provide the plug/barrier potentials.[8] In these experiments, however, it is not elucidated whether the plug/barrier potentials are formed when an ECR point is located in a gradient region of a magnetic field in the absence of magnetic well. In order to clarify essential features of the problem, it is important to make investigations on detailed potential structure due to local ECR under rather simplified configurations.

In this paper, measurements are performed on barrier/plug potentials in the presence of the single ECR point located in a gradient region of a simple converging magnetic field. The potential profiles are demonstrated to be formed, depending on a mirror ratio and input microwave power for ECR. In Sec. II, experimental apparatus and methods are described. Experimental results are presented in Sec. III and are discussed in Sec. IV. Conclusions are included in Sec. V.

II. EXPERIMENTAL APPARATUS

A fully-ionized plasma is produced by surface ionization of potassium atoms on a 5.0-cm-diam hot tungsten plate at one end ($z = +160$ cm) of a single-ended Q machine[9,10] under an electron-rich condition, as shown schematically in Fig. 1. Ions are accelerated by a potential drop of the electron sheath just in front of the hot plate which is grounded electrically, together with a 20.8-cm-diam vacuum chamber. Ion flow energy E_{i0} depends on the sheath potential which can be varied by changing the hot-plate power. There is a tungsten grid (0.03-mm-diam wire, 50 mesh/in.) at a distance of 40 cm from the hot plate, which is used as a gate of a plasma-flow injection. In order to inject the plasma flow along the magnetic field, a step potential ϕ_g up to the plasma potential is applied to the grid which is biased negatively with respect to the hot plate.[3]

A small movable Langmuir probe is used to measure a plasma potential ϕ profile in addition to electron temperature T_e and plasma density n_p profiles. Under our conditions, the plasma density n_{p0} is around 1×10^9 cm^{-3}, the electron temperature T_{e0} is approximately 0.2 eV, the ion temperature $T_{i0} \lesssim T_{e0}$ and the

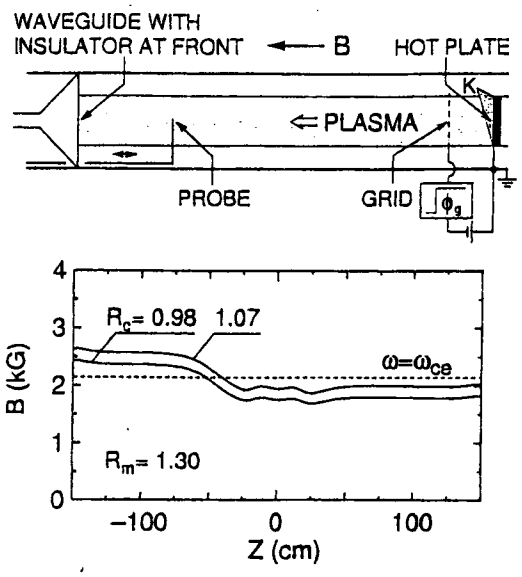

Fig. 1. Schematic of experimental apparatus and converging magnetic-field configuration.

ion flow energy $E_{i0} = 1 \sim 2$ eV. A background gas pressure is 5×10^{-5} Pa. Since the collision mean free paths of electrons and ions are longer than the plasma length under such a condition, the plasma is considered to be collisionless from this point of view. Typical magnetic field configurations are also shown in Fig. 1. The magnetic field has a 50-cm-length gradient region sandwiched between a 170-cm-length and a 80-cm-length flat regions. The magnetic field is changed so as to vary a mirror ratio R_m which is defined as ratio of the magnetic-field strength in the strong region B_m to that in the weak region B_0. A microwave with frequency $\omega/2\pi = 6$ GHz and input power $P_\mu = 0 \sim 1$ W is launched into the plasma through a circular waveguide located on the opposite side of the hot plate. The window of the waveguide is covered with an insulator which terminates the plasma column at $z = -150$ cm. The microwave propagates toward the gradient-field region (ECR region) satisfying the condition $\omega/\omega_{ce} < 1$ and the local ECR takes place at the ECR point (in the vicinity of $\omega/\omega_{ce} = 1$), where $\omega_{ce}/2\pi$ is the electron cyclotron frequency. A subscript "0" stands for the parameters without microwave injection.

In addition to R_m, we define a new parameter $R_C = B_C/B_R$, where B_R and B_C denote magnetic-field strengths at the ECR point and at an inflection point of the magnetic-field line, respectively. The inflection point is roughly determined by calculating $B_C = (B_m + B_0)/2$. According to the definition of R_C, $R_C > 1$ indicates that the field strength at the inflection point is larger than that at the ECR point, namely, the ECR point is located in the bad curvature region. The situation of $R_C < 1$, on the other hand, means that the ECR point is located in the good curvature region. To clarify dynamics of the plasma particles accompanied by the potential formation, we measure spatial and temporal evolutions of the plasma parameters. Here, time resolved measurements are performed by a usual box-car sampling technique.

III. EXPERIMENTAL RESULTS

Figure 2 gives axial plasma potential ϕ profiles at the radial center in the steady state together with electron density n_e and electron temperature T_e profiles with $R_m = 1.30$ and $R_C = 0.98$ for $P_\mu = 0$ W (open marks) and 0.5 W (closed marks). The potential ϕ is almost constant spatially in the upstream region, being independent of P_μ. This constant potential value is a standard against which the spatial variation of ϕ is measured. For $P_\mu = 0$ W, a small increase in ϕ, the hight of which is of the order of T_{e0}/e is observed along the converging magnetic field, agreeing with the result in Ref. 3. For $P_\mu = 0.5$ W, on the other hand,

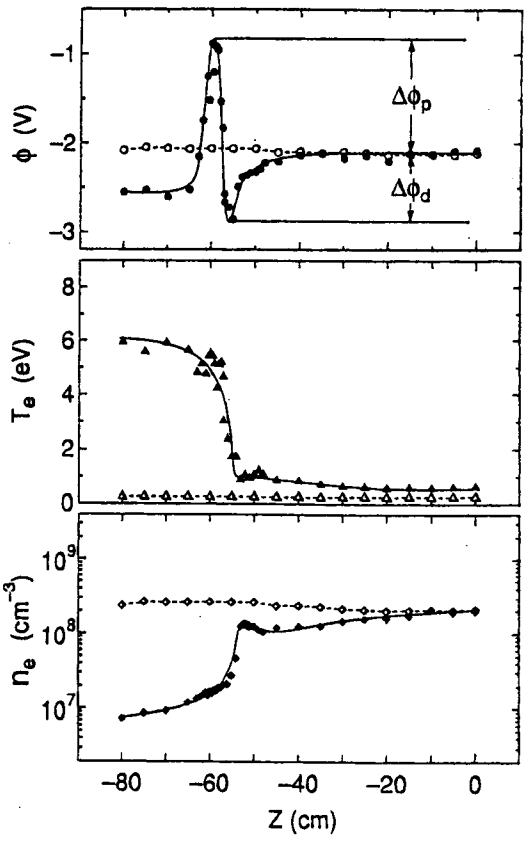

Fig. 2. Spatial profiles of plasma potential ϕ, electron temperature T_e and electron density n_e in the steady state with $R_m = 1.30$ and $R_C = 0.98$ for $P_\mu = 0$ W (open marks) and 0.5 W (closed marks).

there appears a negative potential dip $\Delta\phi_d$ around the ECR region, being accompanied by a drastic positive potential hump $\Delta\phi_p$. Here, $\Delta\phi_p$ and $\Delta\phi_d$ are potential differences from ϕ at $z = 100$ cm. The value of $-\Delta\phi_d$ is about $4T_{e0}/e$, which is enough large to insulate the hot electrons in the ECR region from the cold electrons coming from the source region. The electron temperature T_e increases around the ECR region, and the T_e difference between the upstream and downstream regions is maintained, which demonstrates the $\Delta\phi_d$ function as a thermal barrier. Thus, the potential dip can be called "barrier" potential. The value of $\Delta\phi_p$ is about $7T_{e0}/e$, which is of the order of E_{i0}. Since $\Delta\phi_p$ is able to reflect almost all the ions, the potential hump can be called "plug" potential. The electron density n_e profile for $P_\mu = 0.5$ W shows that a stagnation of electrons is generated in the ECR region and the subsequent steep density drop is formed in the downstream region. These phenomena clearly demonstrate that the plasma is almost plugged by $\Delta\phi_p$, which works as the plug potential. Since the increase in T_e is generated by ECR, the increase in electron temperature perpendicular to the magnetic field $T_{e\perp}$ is expected to be dominant. In order to measure anisotropic T_e a modified directional energy analyzer is used, a collector of which is sensitive to the electron motion perpendicular to the magnetic-field lines. As a result, the T_e increase is confirmed to be mainly caused by the increase in $T_{e\perp}$.

Figure 3 shows $\Delta\phi_p$ as a function of time in the cases of $R_C = 0.98$ and 1.07 with $P_\mu \simeq 0.5$ W and $R_m = 1.30$, where the plasma flow is injected at $t = 0$ msec. For $R_C = 0.98$, it is found that $\Delta\phi_p$ increases as time goes by and persists in the steady state. For $R_C = 1.07$, on the other hand, $\Delta\phi_p$ initially increases

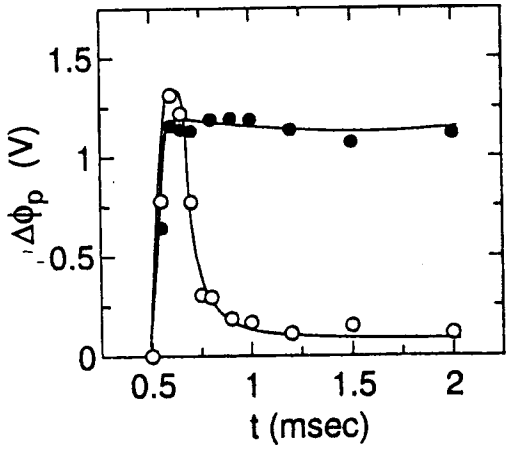

Fig. 3. Potential difference $\Delta\phi_p$ as a function of time with $R_m = 1.30$ for $P_\mu = 0.5$ W. Closed and open circles denote the cases of $R_C = 0.98$ and 1.07, respectively.

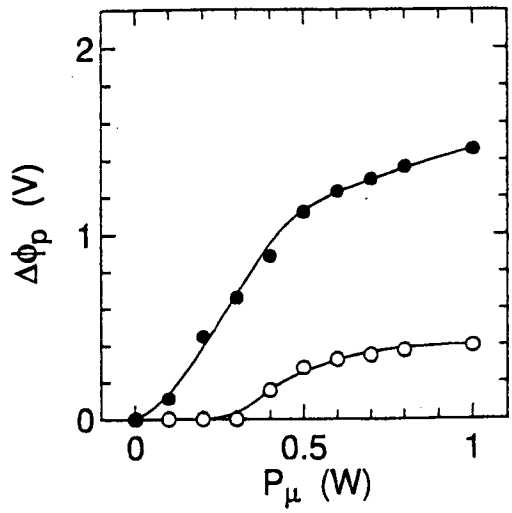

Fig. 4. Potential difference $\Delta\phi_p$ as a function of P_μ in the steady state with $R_m = 1.30$ in the cases of $R_C = 0.98$ (closed circles) and $R_C = 1.07$ (open circles).

and has the maximum value, the hight of which reaches $7T_{e0}/e$ at $t = 0.6$ msec which corresponds to the time necessary for the ion flow to arrive at the ECR region. After that, $\Delta\phi_p$ is observed to decrease gradually and to have a small value ($\simeq T_{e0}/e$) in the steady state. This difference of the $\Delta\phi_p$ evolutions between $R_C = 0.98$ and 1.07 cases is related to low-frequency oscillations, which is described in Sec. IV.

Dependences of $\Delta\phi_p$ on P_μ in the steady state with $R_m = 1.30$ are presented in Fig. 4. For $R_C = 0.98$, the values of $\Delta\phi_p$ apparently increase with an increase in P_μ. For $R_C = 1.07$, however, $\Delta\phi_p$ does not increase and attain to a value much smaller than for $R_C = 0.98$ even if P_μ is increased up to 1 W. At $t = 0.6$ msec, on the other hand, it is experimentally confirmed that $\Delta\phi_p$ for both $R_C = 0.98$ and 1.07 increase in the same way as for $R_C = 0.98$ in the steady state.

Figure 5 gives $\Delta\phi_p$ as a function of R_C with R_m kept constant ($= 1.30$) for $P_\mu = 0.5$ W. At $t = 0.6$ msec, the value of $\Delta\phi_p$ gradually increases with an increase in R_C. Since B_m increases as R_C is increased under the condition that R_m is kept constant, an effective mirror ratio $R_{eff} = B_m/B_R$ rather than $R_m = B_m/B_0$ is closely related to the potential formation when ECR occurs. Thus, the increase in $\Delta\phi_p$ is considered to be caused by the increase in R_{eff}. In the steady state, on the other hand, $\Delta\phi_p$ increases with an increase in R_C in the same way as at $t = 0.6$ msec but suddenly decreases over $R_C \gtrsim 1.0$. According to the definition of R_C, these experimental results indicate that $\Delta\phi_p$ persists in the steady state when the ECR point is located in the good curvature region but $\Delta\phi_p$ collapses in the steady state when the ECR point

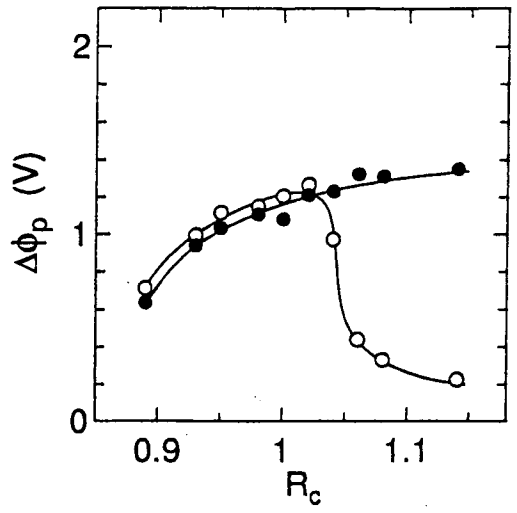

Fig. 5. Potential difference $\Delta\phi_p$ as a function of R_C at $t = 0.6$ msec (closed circles) and in the steady state (open circles) with $R_m = 1.30$ for $P_\mu = 0.5$ W.

is located in the bad curvature region.

In Fig. 6, $\Delta\phi_p$ is plotted as a function of R_m with changing B_m at a fixed value of $B_0 = 1.8$ kG for $P_\mu = 0.5$ W, where R_C is also indicated on the upper abscissa. In this case it is to be noted that R_C simultaneously increases with an increase in R_m. At $t = 0.6$ msec, the value of $\Delta\phi_p$ sharply increases as R_m is increased and gradually saturates for $R_m \gtrsim 1.5$. In the steady state, however, the potential structure is

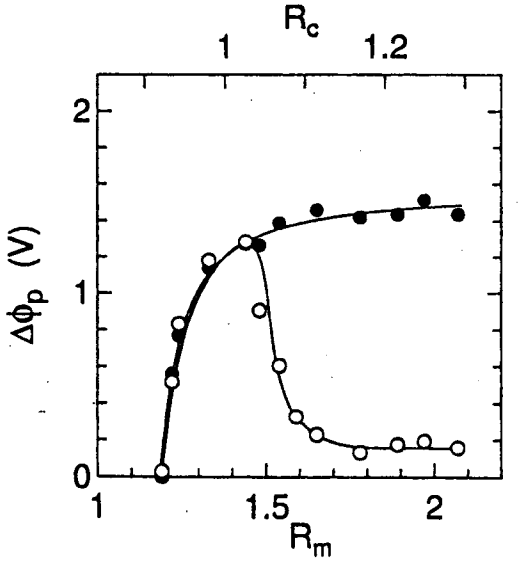

Fig. 6. Potential difference $\Delta\phi_p$ as a function of R_m with changing B_m at a fixed value of $B_0 = 1.80$ kG at $t = 0.6$ msec (closed circles) and in the steady state (open circles) for $P_\mu = 0.5$ W.

observed to collapse over $R_m \gtrsim 1.5$, where R_C exceeds the unity.

IV. DISCUSSIONS

The potential structure is observed to consist of a negative potential dip around the ECR point and a subsequent positive potential hump, as shown in Fig. 2. A physical meaning of the phenomena is as follows. When the plasma arrives at the ECR point, the electrons accelerated perpendicularly to the magnetic field by ECR are axially decelerated and reflected by $-\mu\nabla_\parallel B$ force, where μ is the magnetic moment of electrons and $\nabla_\parallel B$ is the gradient of B in the direction parallel to magnetic field lines. Since the decelerated electrons are stagnated around the ECR point, the potential dip is formed by these stagnated electrons there. On the other hand, the ions are not directly affected by the ECR and might pass through the ECR region. Thus, the positive potential which axially decelerates and reflects the ions is expected to be formed in order to maintain the charge neutrality condition in the resonance and downstream regions. Since $\Delta\phi_p$ reaches about $7T_{e0}/e$ which is equal to the value equivalent of ion flow energy E_{i0}, almost all the ions, which are accelerated by the electron sheath in front of the hot plate, are reflected by this positive potential. As a result, the plasma density decreases in the downstream region owing to the formation of the dike potential against the plasma flow.

As shown in Fig. 4, the value of $\Delta\phi_p$ for $R_C = 0.98$ in the steady state increase with an increase in P_μ. The increase in P_μ enhances the T_e anisotropy, or an increase in $T_{e\perp}$ as already described above. Since the amount of the reflected electrons increases with an increase in $T_{e\perp}$, $\Delta\phi_p$ which is thought to reflect ions increases in order to maintain the charge neutrality condition. Furthermore, $\Delta\phi_p$ always saturates gradually around E_{i0}/e, plugging most of the ions not to pass through the magnetic gradient.

In Fig. 5 and Fig. 6, $\Delta\phi_p$ increases with an increase in R_C or R_m. Judging from our scenario of the potential formation due to ECR, the effective mirror ratio $R_{eff}(= B_m/B_R)$ is a key parameter which links $\Delta\phi_p$ with magnetic-field strength. In Fig. 7, $\Delta\phi_p$ is plotted as a function of R_{eff} in the cases of changing R_C at a fixed value of R_m (closed circles) and changing R_m at a fixed value of B_0 (open circles). $\Delta\phi_p$ increases with an increase in R_{eff} and saturates around E_{i0}/e in the same way in both cases. This result clearly demonstrates that the increase in R_{eff}, or the decrease in a loss-cone angle enhances the electron stagnation around the ECR point, and thus, $\Delta\phi_p$ reasonably increases under the charge neutrality condition.

Figure 3 shows that the potential structure is sus-

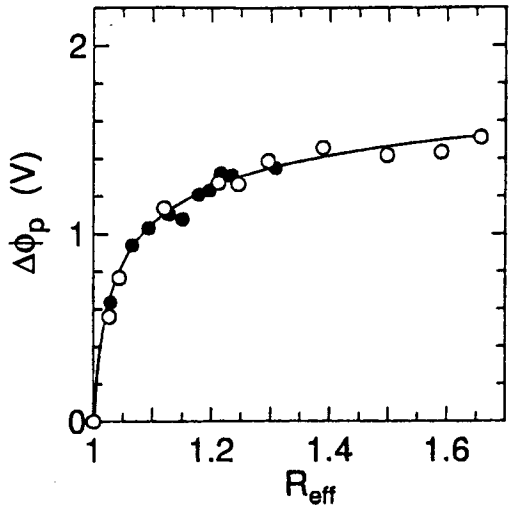

Fig. 7. Potential difference $\Delta\phi_p$ as a function of R_{eff} at t = 0.6 msec for P_μ = 0.5 W in the case of changing R_C at a fixed value of R_m (closed circles) and changing R_m at a fixed value of B_0 (open circles).

tained in the steady state for $R_C < 1$, while the potential structure for $R_C > 1$ gradually collapses as time goes by. The $\Delta\phi_p$ dependence on R_C is given in detail in Fig. 5. It is experimentally confirmed that drift type and fluit type instabilities are observed to be enhanced when the ECR point is located in the region of bad curvature, i.e. in the case of $R_C > 1$. These low-frequency instabilities seem to induce the plasma diffusion in the radial direction and the collapse of the potential structure. This collapse phenomenon agrees with the experimental results under the magnetic-well configuration,[8] where ECR point is located at the bottom of the magnetic-well in the bad curvature region. In the case of $R_C < 1$ the instabilities are suppressed to some extent but still remain, which is considered to result in the density decrease over the whole plasma column as shown in Fig. 2.

V. CONCLUSIONS

Potential profiles are measured in a collisionless plasma flow along a simple converging magnetic field in the presence of the single ECR point. The potential structure observed consists of the negative potential dip $\Delta\phi_d$ around the ECR point and the subsequent positive potential hump $\Delta\phi_p$. $\Delta\phi_d$ is about $-4T_{e0}/e$ which insulates the hot electrons from the cold electrons coming from the source region, and $\Delta\phi_p$ reaches the value equivalent of the ion flow energy (E_{i0}), which plugs almost all the ions. A combination of $\Delta\phi_p$ and $\Delta\phi_d$ results in diking the plasma flow. Although the potential structure in the case of $R_C < 1$ persists in the steady state, the potential structure in the case of $R_C > 1$ temporally collapses as low-frequency flute and drift instabilities are observed to grow. Our experiment has demonstrated a clear mechanism for potential formation due to local ECR under the situation that the ECR point is located in the gradient region of the quite simple configurations of magnetic field. This mechanism could be applied for the understanding potential profiles in complicated situations such as in tandem-mirror devices.

ACKNOWLEDGEMENTS

The authors are indebted to H. Ishida for his technical assistance.

REFERENCES

1. H.Alfvén and C.-G. Fälthammar, *Cosmical Electrodynamics* , 2nd ed., p. 162, Oxford University Press, London (1963).
2. Y. Serizawa and T. Sato, "Formation of a Large-Scale Potential Structure along a Mirror Field Resulting from Parallel Plasma Flows," *Phys. Fluids*, **29**, 2753 (1986).
3. N. Sato *et al.*, "Potential Formation in a High-Speed Plasma Flow along Converging Magnetic Field Lines," *Phys. Rev. Lett.*, **61**, 1615 (1988).
4. G. I. Dimov *et al.*, "Thermonuclear Confinement System with Twin Mirror Systems," *Sov. J. Plasma Phys.*, **2**, 326 (1976).
5. D. P. Grubb *et al.*, "Thermal-Barrier Production and Identification in a Tandem Mirror," *Phys. Rev. Lett.*, **53**, 783 (1984).
6. M. Inutake *et al.*, "Thermal Barrier Formation and Plasma Confinement in the Axisymmetrized Tandem Mirror GAMMA 10," *Phys. Rev. Lett.*, **55**, 939 (1985).
7. T. Tamano, "Tandem Mirror Experiments in GAMMA 10," *Phys. Plasmas* **2**, 2321 (1995).
8. T. Kaneko *et al.*, "Potential Structure Modified by Electron Cyclotron Resonance in a Plasma Flow along Magnetic Field Lines with Mirror Configuration," *Phys. Rev. Lett.*, **80**, 2602 (1998).
9. R. W. Motley, *Q-Machines*, Academic Press, New York (1975).
10. N. Sato *et al.*, "Spatial Evolution of Velocity-Modulated Ion Beams in a Plasma," *Phys. Rev. Lett.*, **34**, 931 (1975).

添付資料 III （発散型磁場配位）

PLASMA POTENTIAL FORMATION AND PARTICLE ACCELERATION DUE TO ECRH IN DIVERGING MAGNETIC-FIELD LINES

Rikizo Hatakeyama
Graduate School of Engineering
Tohoku University
Sendai 980-8579, Japan
+81-22-217-7045

Toshiro Kaneko
Graduate School of Engineering
Tohoku University
Sendai 980-8579, Japan
+81-22-217-7129

Noriyoshi Sato
Graduate School of Engineering
Tohoku University
Sendai 980-8579, Japan
+81-22-217-7112

ABSTRACT

A plasma potential formation is investigated in a fully ionized collisionless plasma flow in the presence of electron cyclotron resonance (ECR) heating (ECRH) under simple diverging magnetic-field configurations. When ECR takes place in a diverging region, there appears a strong potential drop along the field lines, which results from a field-aligned electron acceleration, being accompanied by an effective ion acceleration so as to maintain the charge neutrality condition in the downstream region. Time-resolved measurements are performed in order to clarify dynamics of the potential formation.

I. INTRODUCTION

Charged particle acceleration by $-\mu\nabla_{\parallel}B$ force in plasmas has been recognized to be a basically important process in conjunction with ion conic formation in the ionosphere,[1,2] expansion of the solar wind,[3] plasma thrust[4] and ion impinging in reactive plasma processing,[5] where μ and $\nabla_{\parallel}B$ are magnetic moment increased by various kinds of heating mechanisms and field gradient parallel to magnetic field lines, respectively. Since a heating method or mechanism applied in these investigations predominantly heat electrons or ions, the resultant force of $-\mu\nabla_{\parallel}B$ is expected to induce charge separation, leading to a plasma potential formation along inhomogeneous magnetic-field lines.[6] This viewpoint plays a crucial role, for example, in discussing details of the ion conic formation mechanism such as heating perpendicular to magnetic-field lines and upwelling of the plasma along the auroral field lines.[1,2] To our knowledge, however, no clear-cut experimental result on a relation between $-\mu\nabla_{\parallel}B$ charged-particle acceleration and potential formation has been reported. Here our concern is to clarify details of the potential formation and a relation between potential structure and $-\mu\nabla_{\parallel}B$ particle acceleration due to local electron cyclotron resonance (ECR) heating (ECRH).

In this paper, measurements are performed on a potential formation accompanied by particle acceleration in the presence of the single ECR point located in a gradient region of a simple diverging magnetic field. In Sec. II, an experimental apparatus and methods are described. Experimental results and discussions are presented in Sec. III. Conclusions are included in Sec. IV.

II. EXPERIMENTAL APPARATUS

The experiment is performed with a fully-ionized plasma which is produced by surface ionization of potassium atoms on a 6.0-cm-diam hot tungsten plate at one end ($z = +160$ cm) of a single-ended Q machine[7,8] under an electron-rich condition, as shown schematically in Fig. 1. Ions are accelerated by a potential drop of the electron sheath just in front of the hot plate which is grounded electrically, together with a 20.8-cm-diam vacuum chamber. Ion flow energy E_{i0} depends on the sheath potential which can be varied by changing the hot-plate power. There is a tungsten grid (0.03-mm-diam wire, 50 mesh/in.) at a distance of 40 cm from the hot plate, which is used as a gate to inject a plasma flow. To the grid which is biased negatively with respect to the hot plate, a step potential ϕ_g up to the plasma potential is applied in order to inject the plasma flow along the magnetic field.

A small movable Langmuir probe is used to measure plasma parameters including an electron energy distribution function and their axial profiles. An ion energy distribution function is measured by a directional electrostatic energy analyzer. Under our conditions, the plasma density n_{p0} is around 1×10^9 cm^{-3}, the electron temperature T_{e0} is approximately 0.2 eV, the ion temperature $T_{i0} \lesssim T_{e0}$ and the ion flow energy $E_{i0} \simeq 2$ eV. A background gas pressure is 5×10^{-5} Pa. Under such a condition, the collision mean free paths

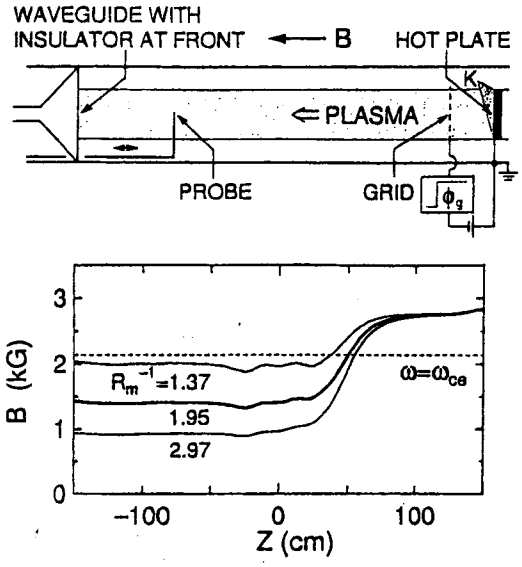

Fig. 1. Schematic of experimental apparatus and diverging magnetic-field configuration.

of electrons and ions are longer than the plasma length and, from this point of view, the plasma is collisionless. Typical diverging magnetic-field configurations are shown in Fig. 1. The magnetic field has a 50-cm-length gradient region sandwiched between a 80-cm-length and a 170-cm-length flat regions. The magnetic field is changed so as to vary the degree of field divergence R_m^{-1} (reciprocal of so-called mirror ratio R_m) in the range of $1 \sim 3$, which is defined as ratio of the magnetic-field strength in the strong region to that in the weak region.

A microwave with frequency $\omega/2\pi = 6$ GHz and input power $P_\mu = 0 \sim 1$ W is launched into the plasma through a circular waveguide located on the opposite side of the hot plate. A waveguide window is covered with an insulator which terminates the plasma column at $z = -150$ cm. The microwave propagates toward an ECR point ($\omega = \omega_{ce}$) from the weak to the strong magnetic-field strength regions, where $\omega_{ce}/2\pi$ is the electron cyclotron frequency. In this situation, the wave approaches the ECR point from its cutoff-point side, and the wave amplitude might decrease in the evanescent region. In our experimental condition of low n_{p0}, however, the evanescent region is very narrow ($\simeq 0.1$ cm) in comparison with the wave length ($= 5$ cm) because of the condition $\omega_{pe} \ll \omega_{ce}$, where $\omega_{pe}/2\pi$ is the electron plasma frequency. Thus, the wave passes through the evanescent region by a tunneling effect[9,10] and ECR can take place beyond the cutoff point. A subscript "0" stands for the parameters without microwave injection. To clarify dynamics of the plasma particles accompanied by the potential formation, we measure spatial and temporal evolutions of the plasma parameters. Here, time resolved measurements are performed by a usual box-car sampling technique.

III. EXPERIMENTAL RESULTS AND DISCUSSIONS

Measurements of axial profiles of plasma potential ϕ, electron density n_e and electron temperature T_e at the radial center are performed in the steady state with $R_m^{-1} = 1.95$ for $P_\mu = 0$ W (open marks) and $P_\mu = 0.5$ W (closed marks) as shown in Fig. 2. Here, arrows at $z = 50$ cm indicate the position of ECR point. ϕ is almost constant spatially in the upstream region for both $P_\mu = 0$ W and 0.5 W. In the downstream region from the ECR point, on the other hand, ϕ strongly decreases along the plasma flow for $P_\mu = 0.5$ W. This profile is similar to that of the magnetic-filed strength. The absolute value of this potential drop $|\Delta\phi|$, which is the potential difference between the upstream ($z = 100$ cm) and downstream ($z = -100$ cm) regions, is more than 15 V. The po-

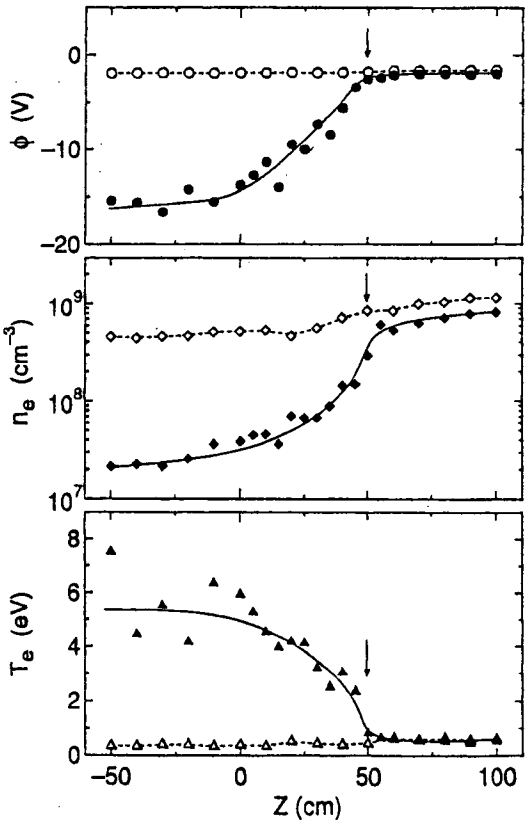

Fig. 2. Spatial profiles of plasma potential ϕ, electron density n_e and electron temperature T_e in the steady state with $R_m^{-1} = 1.95$ for $P_\mu = 0$ W (open marks) and 0.5 W (closed marks).

tential drop $\Delta\phi$ is expected to lead to the acceleration of ions towards the downstream region as will also be described later. n_e decreases along the magnetic-field lines even for $P_\mu = 0$ W, and n_e in the downstream region becomes 40 % of that in the upstream region. This is because the cross section of plasma column in the downstream region becomes about twice that in the upstream region in the case of $R_m^{-1} \simeq 2$ and the amount of electron acceleration parallel to the magnetic field attains to 1.2 times by transferring the perpendicular energy of the isotropic electrons to the parallel energy. For $P_\mu = 0.5$ W, on the other hand, n_e drastically decreases beyond the ECR point, where n_e is smaller than n_{e0} by an order of magnitude. This decrease in n_e will be discussed in the present section in connection with the drop of ϕ. T_e in the downstream region from the ECR point increases along the magnetic-field lines for $P_\mu = 0.5$ W. $T_e \simeq 30T_{e0}$ is attained at $z = -50$ cm, which is caused by the heating due to ECR and the conversion of the perpendicular energy into the parallel energy.

The electron energy distribution function $F_e(V_c)$ and ion energy distribution function parallel to the magnetic field $F_{i\parallel}(V_c)$ are obtained from the first derivatives dI_c/dV_c,[11] where I_c is the current flowing to the probe or a collector of the energy analyzer and V_c is the voltage of the probe or the collector applied with respect to the hot plate. Axial variations of $F_e(V_c)$ and $F_{i\parallel}(V_c)$ with $R_m^{-1} = 1.95$ are typically shown in Fig. 3, where both the peak heights are adjusted to the same value because our attention is focused on V_c yielding the peaks. $F_e(V_c)$ and $F_{i\parallel}(V_c)$ for $P_\mu = 0$ W are almost the same in the upstream ($z = 100$ cm) and downstream ($z = -35$ cm) regions [Fig. 3(a)]. Here V_c yielding the peak of $F_e(V_c)$ indicates the plasma potential ϕ ($\simeq -2$ V) which coincides with the result in Fig. 2. V_c yielding the peak of $F_{i\parallel}(V_c)$ shifts from that of $F_e(V_c)$ toward the positive value of V_c by about 2 V. This difference of V_c shows that the initial ion flow energy $E_{i0} \simeq 2$ eV is generated by the electron sheath in front of the hot plate. No appreciable difference of $F_e(V_c)$ and $F_{i\parallel}(V_c)$ in the upstream region is found between the cases of $P_\mu = 0$ W and 0.5 W. In the downstream, on the other hand, $F_e(V_c)$ is measured to

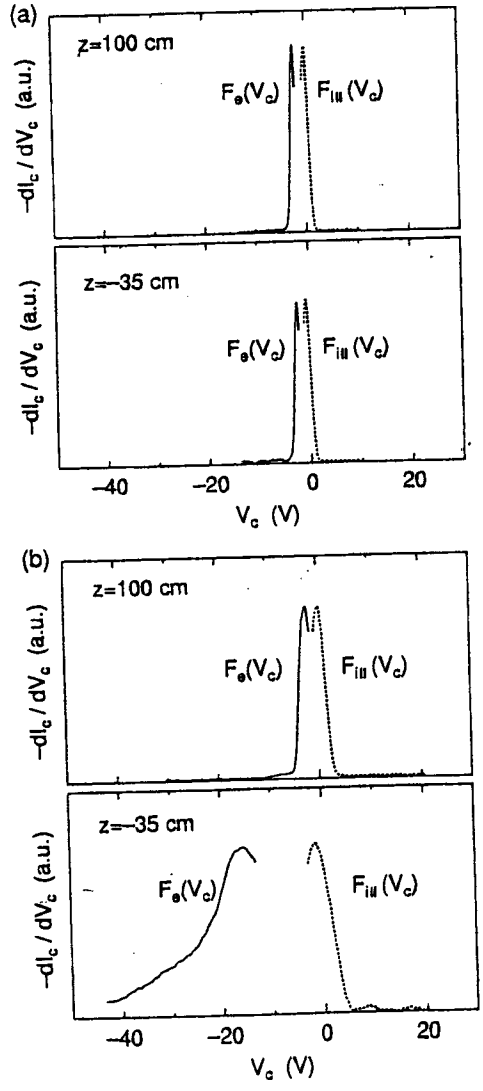

Fig. 3. Energy distributions of electrons $F_e(V_c)$ and ions parallel to the magnetic field $F_{i\parallel}(V_c)$ in the steady state with $R_m^{-1} = 1.95$ for (a) $P_\mu = 0$ W and (b) $P_\mu = 0.5$ W at typical axial positions.

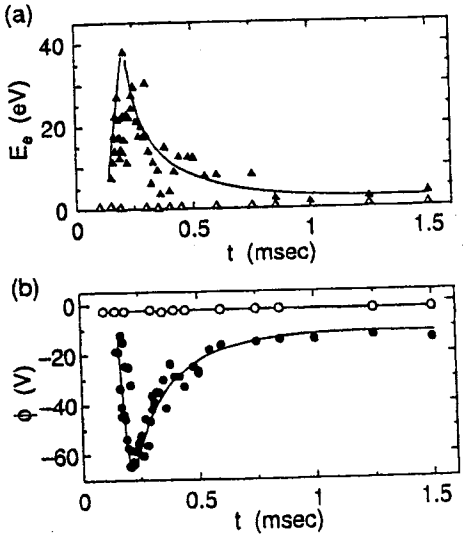

Fig. 4. (a)Average electron energy E_e and (b) plasma potential ϕ as a function of time with $R_m^{-1} = 1.95$ for $P_\mu = 0.5$ W. Open and closed marks denote values at $z = 100$ cm and $z = -100$ cm, respectively.

greatly shift to the negative value of V_c and to consist of electrons with a higher temperature of $T_e \simeq 30T_{e0}$ [Fig. 3(b)]. This peak shift corresponds to the plasma potential drop $|\Delta\phi| \simeq 15$ V in Fig. 2. Since V_c yielding the peak of $F_{i\parallel}(V_c)$ does not change even in the downstream region, i.e., it relatively shifts from the plasma potential (the peak of $F_e(V_c)$) toward the largely positive value of V_c, the ions turn out to have a directional energy parallel to the magnetic field, forming the ion beam flowing downstream. The parallel ion energy E_i, which is defined as the V_c difference between the peaks of $F_e(V_c)$ and $F_{i\parallel}(V_c)$, is found to be nearly equal to the value equivalent of $|\Delta\phi|$. Judging from the above, the ion acceleration is closely related to the potential formation.

In order to clarify dynamics of the potential formation, time-resolved measurements of (a) average electron energy E_e and (b) plasma potential ϕ after injection of the plasma flow at $t = 0$ msec are performed for $P_\mu = 0.5$ W at $z = 100$ cm (open marks) and $z = -100$ cm (closed marks), as shown in Fig. 4. Here we apply the average electron energy E_e instead of the electron temperature T_e, which is obtained from the slope of the semi-log plots of the $I_c - V_c$ characteristics in the tail region of the electron distribution, because the electron energy distribution is not thermalized in this time scale after perpendicular heating by ECR and energy transformation through $-\mu\nabla_\parallel B$ force. Thus E_e and T_e are used in the temporal and steady state cases, respectively. When a front of the plasma-flow pulse arrives around the ECR point ($t = 0.15$ msec), E_e in the region downstream from the ECR point is measured to be extremely high up to $E_e/T_{e0} > 10^2$, which is due to proceeding electrons heated by ECR, while almost no change of E_e is observed in the upstream region. In this case, ϕ in the downstream region is measured to become extremely negative while there is no change of ϕ in the upstream region, where the spatial difference between them attains to $|\Delta\phi| \gtrsim 60$ V. As the bulk plasma continuously passes through the ECR point ($t \gtrsim 0.23$ msec), E_e and $|\Delta\phi|$ gradually decrease, approaching a steady state ($|\Delta\phi| \simeq 15$ V, $T_e \simeq 5$ eV). It can be seen from this figure that the decrease and the increase in ϕ correspond to the increase and the decrease in E_e, respectively.

Figure 5 presents a temporal evolution of axial ϕ profile for $P_\mu = 0.5$ W. A kind of ambipolar potential with a large potential difference ($e|\Delta\phi|/T_{e0} > 10^2$) is

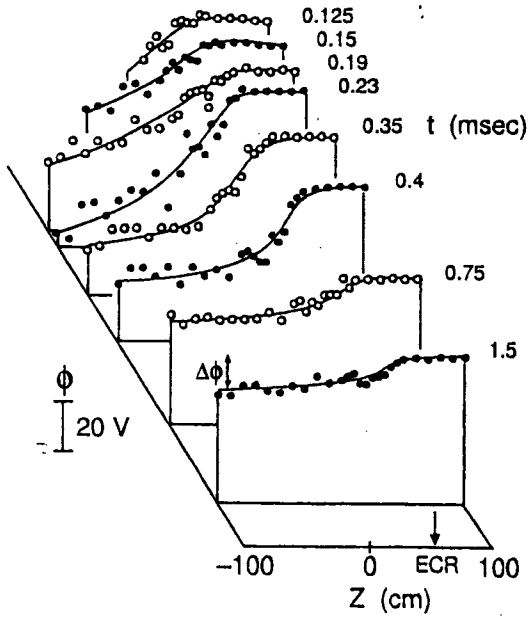

Fig. 5. Temporal evolution of axial plasma potential profile ϕ after the plasma flow is injected at $t = 0$ msec with $R_m^{-1} = 1.95$ for $P_\mu = 0.5$ W.

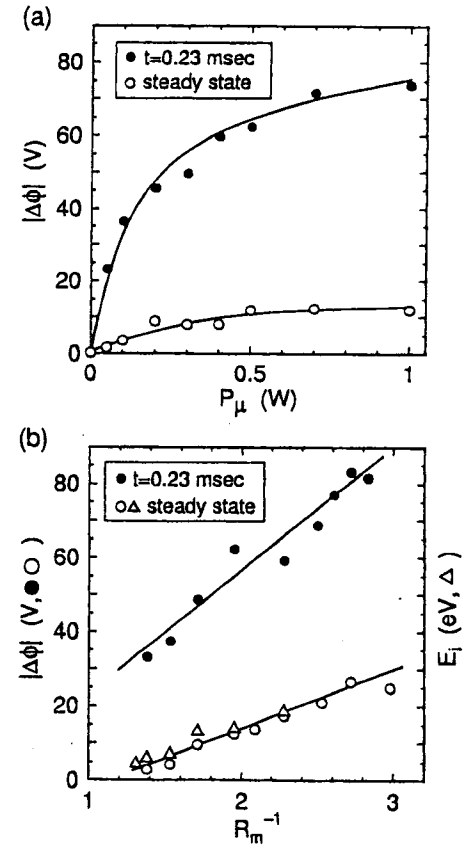

Fig. 6. Potential differences $|\Delta\phi|$ (circles) and parallel ion energy E_i (triangles) (a) as a function of P_μ with $R_m^{-1} = 1.95$ and (b) as a function of R_m^{-1} for $P_\mu = 0.5$ W. Closed and open marks denote values at $t = 0.23$ msec and in the steady state, respectively.

observed to extend over a long distance towards the region downstream from the ECR point when the ECR of front electrons in the expanding plasma is initiated ($t \lesssim 0.23$ msec). Then the potential gradient is found to be localized ahead of the ECR point, the potential drop $\Delta\phi$ to be gradually filled up after the arrival of the bulk electrons ($t \gtrsim 0.23$ msec) and the steady state potential structure is finally formed ($t \gtrsim 1$ msec).

In Fig. 6(a), $|\Delta\phi|$ at $t = 0.23$ msec and in the steady state are plotted as a function of P_μ with $R_m^{-1} = 1.95$. Both transient and steady state $|\Delta\phi|$ increase with an increase in P_μ, being followed by a gradual saturation. In this case, E_e at $t = 0.23$ msec and T_e in the steady state in the downstream region increase in a quite similar way to $|\Delta\phi|$, which indicates that $|\Delta\phi|$ is closely related to E_e and T_e. Dependences of $|\Delta\phi|$ on R_m^{-1} at $t = 0.23$ msec and in the steady state for $P_\mu = 0.5$ W are presented in Fig. 6(b). The potential drops are linearly enhanced with an increase in R_m^{-1}. According to measurements of the ion energy parallel to the magnetic field lines E_i in the steady state (see Fig. 3), it is found that ions are greatly accelerated along the field lines to attain to E_i corresponding to $e|\Delta\phi|$ (open triangles). In this figure, E_i is observed to be larger than $e|\Delta\phi|$ by a few eV, which can be explained by adding the initial ion flow energy $E_{i0} \simeq 2$ eV to the value equivalent of potential drop $e|\Delta\phi|$.

Let us briefly mention the mechanism of the potential formation. As described above, the large potential drop is observed in the region downstream from the ECR point under the diverging-field configuration. At the ECR point, the electrons are accelerated by the ECR in the direction perpendicular to the magnetic field, and are accelerated in the axial direction by $-\mu\nabla_\parallel B$ force along the magnetic-field lines. n_e in the downstream region drastically decreases as shown in Fig. 2 because of the conservation of the electron flux, while ions are not directly affected by the ECR. Thus, the strong ambipolar potential leading to the ion acceleration is considered to be formed so as to maintain the charge neutrality condition in the region downstream from the ECR point.

When P_μ and R_m^{-1} are increased, the electron energy perpendicular to the magnetic field increases and the conversion of the perpendicular energy into the parallel energy is enhanced, which cause the increase in the electron energy parallel to the magnetic-field lines. Thus, the potential drop $|\Delta\phi|$ which accelerates the ion along the magnetic field is selfconsistently increased.

IV. CONCLUSIONS

Our experiment demonstrates that the local ECR in the diverging magnetic field results in the formation of the strong potential drop along the field lines, which is promoted by field-aligned electron acceleration leading to effective ion acceleration so as to maintain the charge neutrality condition downstream from the ECR point. Furthermore, it is clarified that the average electron energy and the potential drop transiently increase by several times that in the steady state. This work could give useful ideas to clarify the mechanism of the ion conic formation and to control the ion energy accelerated by the potential drop due to local ECR.

ACKNOWLEDGEMENTS

The authors are indebted to H. Shoji and K. Kojima for their collaborations in the preliminary measurements and H. Ishida for his technical support.

REFERENCES

1. S. L. Cartier *et al.*, "A Laboratory Study of Ion Energization by EIC Waves and Subsequent Upstreaming along Diverging Magnetic Field Lines," *J. Geophys. Res.*, **91**, 8025 (1986).
2. M. Zintl *et al.*, "Transverse Ion Acceleration and Ion Conic Formation in a Divergent-Field Laboratory Plasma," *Phys. Plasmas*, **2**, 4432 (1995).
3. R. E. Hartle and P. A. Sturrock, "Two-Fluid Model of the Solar Wind," *Astrophys. J.*, **151**, 1155 (1968).
4. E. B. Hooper, Jr., "Plasma Flow Resulting from Electron Cyclotron Resonance Heating on a Magnetic Hill," *Phys. Plasmas*, **2**, 4563 (1995).
5. Y. Okuno *et al.*, "Two-Dimensional Ion Velocity Distribution Function in Electron Cyclotron Resonance Plasma under a Divergent Magnetic Field," *J. Appl. Phys.*, **74**, 5990 (1993).
6. R. Geller *et al.*, "Electric Fields Parallel to the Magnetic Field in a Laboratory Plasma in a Magnetic Mirror Field," *J. Plasma Phys.*, **12**, 467 (1974).
7. R. W. Motley, *Q-Machines*, Academic Press, New York (1975).
8. N. Sato *et al.*, "Spatial Evolution of Velocity-Modulated Ion Beams in a Plasma," *Phys. Rev. Lett.*, **34** 931 (1975).
9. D. B. Batchelor, "Budden Tunnelling in Parallel Stratified Plasmas," *Plasma Phys.*, **22** (1980) 41.
10. R. F. Ellis *et al.*, "Emission, Absorption, and Tunneling of Whistler Waves in an Inhomogeneous Magnetic Field," *Phys. Fluids*, **26** 1528 (1983).
11. R. Hatakeyama *et al.*, "Ion-Energy Distribution in a Plasma under a Diverging Magnetic Field," *J. Appl. Phys.*, **45**, 85 (1974).

添付資料 Ⅳ（波動基礎過程）

プラズマ・核融合学会第16回年会　1999年11月23日～26日　25pA13p

不均一磁場中ECRに関与する波動伝播

Wave Propagation Related to ECR in Inhomogeneous Magnetic Fields

東北大学大学院工学研究科　村井 宏一，金子 俊郎，畠山 力三，佐藤 徳芳

これまで，筆者らのグループによって不均一磁化プラズマ中での電子サイクロトロン共鳴(ECR)に伴うサーマルバリア付きタンデムミラー型電位構造の形成機構が基礎実験により明らかにされてきた．一方，ECRに関与するマイクロ波のプラズマ中での伝播・吸収に関しては，高効率プラズマ生成の観点から大電力投入により生成されたECR放電プラズマ中での減衰の様子等が主に調べられてきている．しかし，これら局所ECRに至る波動の伝播・吸収に関するプラズマ密度，モード，磁場勾配に対する依存性や非線形効果等の詳細な測定は成されておらず，それに伴う電子加熱さらには電位形成への寄与については全く議論されていないのが現状である．そこで本研究では，ECRに関与する波動の伝播・吸収の線形から非線形性への遷移過程を基礎実験的に明らかにするとともに，さらなる非線形発展である電位構造形成に至る機構の理解に有用な知見を得ることを目的としている．

実験は東北大学 Q_T − machine 装置において，外部印加磁場強度 $B \simeq 2.14$ kG(電子サイクロトロン周波数 $f_{ce} = 6$ GHz) 中での熱陰極直流放電プラズマに対してマイクロ波を入射して行った．マイクロ波は発振器から14 mWの出力で，主にヘリカルアンテナを用いて入射した．このヘリカルアンテナは，放射部分の螺旋の回転方向により，磁場に平行な右回り円偏波 (R-mode) 及び左回り円偏波 (L-mode) を選択的にプラズマ中へ入射できる．測定は，軸方向に掃引可能なモノポールアンテナでマイクロ波を受信し，干渉法を用いて行った．

図1は，ヘリカルアンテナによるマイクロ波入射を一様磁場中で行った場合の分散関係 (f:周波数，λ:波長) 及びその時の振幅強度を示している．R-mode及びL-modeでマイクロ波を入射した場合，それぞれ磁場に平行に伝播する電磁波であるR波及びL波の分散関係に従うことが分かった．また振幅強度の周波数依存性より，R- modeのみならず，ECRに関与しないと考えられるL-modeでも周波数 f が f_{ce} に近づくにつれて減衰していくことが明らかになった．

図2は，不均一磁場配位中でのマイクロ波干渉波形である．R-mode励起においては，共鳴点に近づくにつれ，R波の分散関係に従って波長が短くなり，また波動が減衰していく様子を確認できる．一方，L-mode励起の場合，波長は分散関係どおり約5.3 cmでほぼ一定であるが，ECR点付近でやはり波動の減衰が観測される．

またこの減衰は，プラズマ密度や外部印加磁場の勾配長などに依存し，高密度であるほど或いは緩やかな磁場勾配であるほど大きいことが分かった．しかし，その減衰率は理論から予想される値とは大きく異なっており，これまで議論がなかった上述のL-modeでの減衰とともに，僅かに存在する高温電子または中性ガスとの衝突などに起因している可能性がある．

現在，以上のような点をもとに波動の共鳴・減衰・吸収の機構の詳細について検討を進めているが，その結果を踏まえて非線型発展の実験を行う予定である．

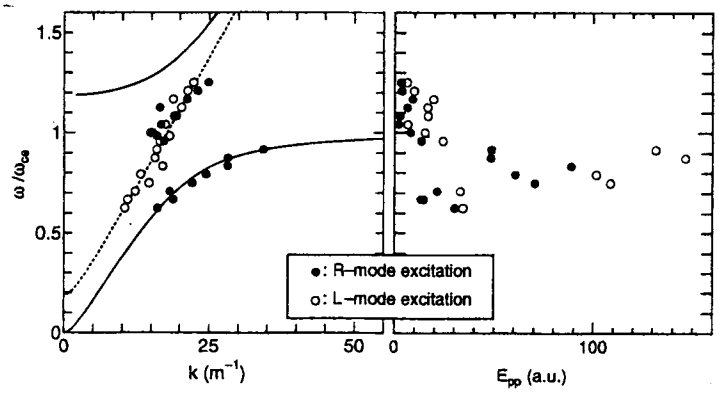

図1: 分散関係及び振幅−周波数特性.

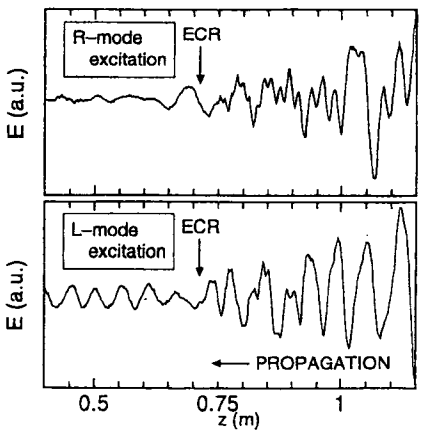

図2: 不均一磁場中干渉波形.